6ICEGE 6th International Conference on Earthquake Geotechnical Engineering
1-4 November 2015
Christchurch, New Zealand

Multi-modal determination of Rayleigh wave dispersion and attenuation curves using the circle fit method

R. Verachtert[1], G. Degrande[2]

ABSTRACT

In a multi-channel analysis of surface waves (MASW) experiment, inversion of Rayleigh wave dispersion and attenuation curves is used to determine the shear wave velocity and material damping ratio of shallow soil layers. Peak picking and the half-power bandwidth method can be used to determine the dispersion and attenuation curves, respectively. In this paper, the circle fit method is proposed to improve the determination of multi-modal dispersion and attenuationn curves. A numerical MASW experiment is simulated for a layered halfspace, corresponding to a site in Lincent (Belgium). It is shown that the circle fit method results in more accurate estimations of multi-modal dispersion curves than peak picking. Both the circle fit and half-power bandwidth method result in reliable attenuation curves of dominant modes. For other modes an alternative more robust measure of attenuation, based on the circle fit method, is proposed which would enable inversion of these modes.

Introduction

Surface wave analysis is frequently used to determine shear wave velocity and damping of shallow soil layers. These dynamic soil properties are important for seismic site characterization, the prediction of ground borne vibrations, determination of soil structure interaction etc. and can be determined by inversion of Rayleigh wave dispersion and attenuation curves. Multi-channel analysis of surface waves (MASW) can be used to obtain these experimental curves (Park et al., 1999; Foti et al., 2011). The solution of the inversion problem, however, is non-unique due to the limited identified frequency range. In order to reduce non-uniqueness, multi-modal inversion of dispersion curves is frequently performed. Multi-modal determination of attenuation curves remains difficult, since most techniques only allow to extract the attenuation of a dominant Rayleigh wave from spatial data (Xia et al., 2002; Foti, 2004; Lai et al., 2002). Recently, a method for estimating the complex wavenumbers of multiple modes has been proposed by Misbah and Strobbia (2014). The half-power bandwith method proposed by Badsar et al. (2010), theoretically, allows the determination of the attenuation of different Rayleigh wave modes, but is only accurate in the case of dominant modes.

In this paper, the circle fit method (Ewins 1984) is applied to improve the determination of multi-modal dispersion and attenuation. This method has originally been developed to determine the eigenfrequencies and modal damping ratio of a structure from the phase information in the frequency response function (FRF) and is considered an improvement to the traditional peak picking and half-power bandwidth method.

[1]PhD student, Department of Civil Engineering, KU Leuven, Leuven, Belgium, ramses.verachtert@bwk.kuleuven.be
[2]Professor, Department of Civil Engineering, KU Leuven, Leuven, Belgium, geert.degrande@bwk.kuleuven.be

To test the method, wave propagation in a multi-layered halfspace with dynamic soil characteristics corresponding to a site in Lincent (Belgium) is studied. In the frequency-wavenumber (fk) domain, closed form expressions of the soil's Green's functions can be formulated. Rayleigh wave dispersion and attenuation curves are defined. The peak picking and half-power bandwidth method for the determination of dispersion and attenuation curves, respectively, are briefly reviewed and the circle fit method is elaborated. In a next step a numerical MASW experiment is performed in order to compare the circle fit method with the peak picking and half-power bandwidth method.

Wave propagation in layered media

Wave propagation in layered media can be studied with the direct stiffness method (Kausel and Roësset, 1981) in the fk-domain, as implemented in the ElastoDynamics Toolbox (EDT) (Schevenels et al., 2009). The displacements $\widetilde{\boldsymbol{U}}(k_r,\omega)$ relate to the applied loads $\widetilde{\boldsymbol{P}}(k_r,\omega)$ by:

$$\widetilde{\boldsymbol{K}}(k_r,\omega)\widetilde{\boldsymbol{U}}(k_r,\omega) = \widetilde{\boldsymbol{P}}(k_r,\omega). \tag{1}$$

The stiffness matrix $\widetilde{\boldsymbol{K}}(k_r,\omega)$ depends on the Lamé coefficients μ and λ, or the shear wave velocity C_s and dilatational wave velocity C_p, the material damping ratios β_s and β_p of the shear and dilatational waves, the density ρ and the thickness d of each soil layer. Material damping is assumed to be rate independent in the low frequency range and small, allowing the application of the correspondence principle (Rizzo and Shippy, 1971), valid for small damping ratio's. This principle results in the use of complex Lamé coefficients $\mu(1+2\beta_\mathrm{s}\mathrm{i})$ and $(\lambda+2\mu)(1+2\beta_p\mathrm{i})$.

Table 1. Dynamic soil characteristics of the site in Lincent.

layer	d [m]	C_s [m/s]	C_p [m/s]	β_s [-]	β_p [-]	ρ [kg/m³]
1	1.4	128	286	0.044	0.044	1800
2	2.7	176	286	0.038	0.038	1800
3	∞	355	1667	0.037	0.037	1800

A multi-layered halfspace with dynamic soil characteristics retrieved from an MASW experiment at a site in Lincent (Belgium) (Table 1), is subsequently considered. It was assumed that $\beta_\mathrm{s}=\beta_p$ and C_p was determined from first arrival times of the body waves. A load vector $\widetilde{\boldsymbol{P}}(k_r,\omega)$ corresponding to a Dirac impulse in space and time is applied at the surface, resulting in a displacement field $\tilde{u}_{iz}^{G}(k_r,z,\omega)$, denoted as a Green's function or fundamental solution. Figure 1a shows the modulus of the vertical displacement $\tilde{u}_{zz}^{G}(k_r,\omega)$, along the surface $z=0$, normalized for each frequency, as a function of frequency ω and phase velocity $C_r=\omega/k_r$. The peaks in the spectrum correspond to the Rayleigh wave modes. Rayleigh waves are free surface waves with complex wavenumbers k_R, which are solutions of the eigenvalue problem:

$$\det\,\widetilde{\boldsymbol{K}}(k_r,\omega) = 0. \tag{2}$$

The roots k_R can be determined by a search algorithm which minimizes

det $\widetilde{\boldsymbol{K}}(k_r, \omega)$ in terms of the complex wavenumber k_r. The theoretical Rayleigh wave phase velocity of the j^{th} mode is obtained as $C_{\text{R}j}^{\text{T}} = \omega/\text{Re}(k_{\text{R}j}^{\text{T}})$. Figure 1b shows $C_{\text{R}j}^{\text{T}}$ $(j = 1, 2)$. C_{R1}^{T} varies from the Rayleigh wave velocity of the underlying half space at limiting low frequencies, to the Rayleigh wave velocity of the surface layer at limiting high frequencies. C_{R2}^{T} only exists for frequencies above 14 Hz and varies from the shear wave velocity of the underlying half space at limiting low frequencies, to the shear wave velocity of the surface layer at limiting high frequencies. For high frequencies this mode is less dominant.

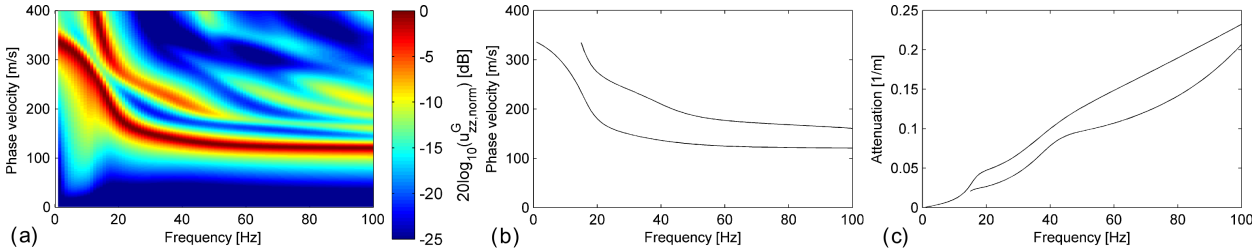

Figure 1. (a) Theoretical fk-spectrum of the Green's function at the site in Lincent. Rayleigh wave (b) phase velocity $C_{\text{R}j}^{\text{T}}$ and (c) attenuation $A_{\text{R}j}^{\text{T}}$ curves, $(j = 1, 2)$.

The attenuation coefficient is calculated as $A_{\text{R}j}^{\text{T}} = -\text{Im}(k_{\text{R}j})$. Figure 1c shows the attenuation curves of the first two modes. At low frequencies, A_{R1}^{T} is mainly determined by the material damping of the underlying halfspace. At higher frequencies, when the penetration depth of the waves is smaller, A_{R1}^{T} is more influenced by the top layers.

Figure 2a shows the modulus of the Green's function $\tilde{u}_{zz}^{G}(k_r, \omega)$ at 50 Hz. The peaks can be picked (at $k_{\text{R}j}^{\text{Tp}}$) to estimate the Rayleigh wave phase velocity $C_{\text{R}j}^{\text{Tp}} = \omega/k_{\text{R}j}^{\text{Tp}}$. The maximum modulus is obtained at $k_{\text{R1}}^{\text{Tp}}$, marked red. Figure 3a shows $C_{\text{R}j}^{\text{Tp}}$ $(j = 1, 2)$ up to 100 Hz. A good correspondence is found with $C_{\text{R}j}^{\text{T}}$.

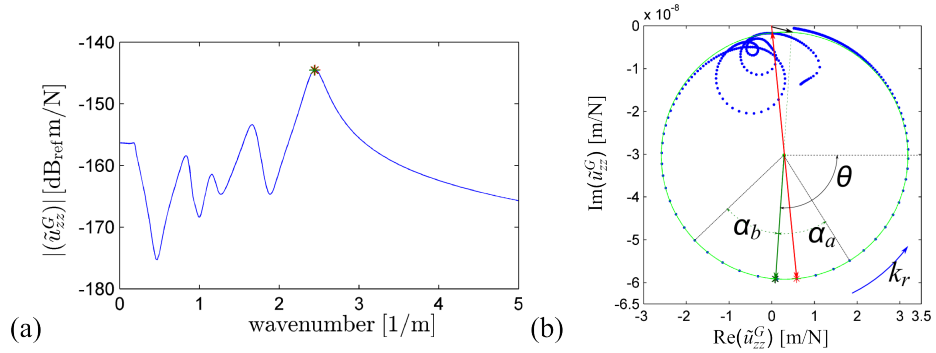

Figure 2. (a) Modulus and (b) Nyquist plot of the Green's function $\tilde{u}_{zz}^{G}(k_r, \omega)$ at 50 Hz.

The width of the peak is influenced by the attenuation of the Rayleigh wave mode. Badsar et al. (2010) assume that the Green's function in the neighbourhood of the peak is similar to the FRF of a single degree of freedom (SDOF) system. In the case of hysteretic damping, the dimensionless FRF of a SDOF system can be written as:

$$\widehat{H}(\omega) = \frac{1}{1-(\omega/\omega_{\mathrm{n}})^2+2\xi\mathrm{i}'} \tag{3}$$

where ω_{n} is the natural frequency of the undamped system and ξ is the damping ratio. The pole ω_{f} of this equation, which corresponds to the free vibration frequency is calculated as:

$$\omega_{\mathrm{f}} = \omega_{\mathrm{n}}\sqrt{1+2\xi\mathrm{i}} \approx \omega_{\mathrm{n}}(1+\xi\mathrm{i})\,, \tag{4}$$

where the last approximation holds for small ξ. At the natural frequency the FRF reaches a maximum. The location of the maximum can thus be used to identify the real part of the free vibration frequency of the system. The damping of lightly damped structures can be obtained by a generalized form of the half-power bandwidth method:

$$\xi = \frac{\Delta\omega}{2\omega_n\sqrt{\gamma^{-2}-1}}. \tag{5}$$

$\Delta\omega$ is defined as the width of the peak where the magnitude of the FRF is γ times the peak value. Badsar et al. (2010) recommend a value of $\gamma = 0.99$ to avoid mixing of neighbouring peaks in the case of multiple Rayleigh wave modes. Under the assumption that the Green's function at the surface is dominated by the presence of clearly separated Rayleigh wave modes, without significant influence of other wave types, a good approximation of the Green's function in the neighbourhood of the j^{th} Rayleigh wave mode is:

$$\tilde{u}_{zz}^{G}(k_r,\omega) \simeq \frac{C_1(\omega)}{1-\left(k_r/\mathrm{Re}(k_{\mathrm{R}j}(\omega))\right)^2+2\xi_{\mathrm{R}j}(\omega)\mathrm{i}} + C_2(\omega), \tag{6}$$

where $\xi_{\mathrm{R}j}(\omega) = A_{\mathrm{R}j}/k_{\mathrm{R}j}$ is the damping ratio of the j^{th} Rayleigh wave and $C_1(\omega)$ and $C_2(\omega)$ are (complex) constants, which depend on the damping and other wave modes. In the remainder of the paper, the frequency dependence will be implicitly assumed. If C_2 is sufficiently small, the Rayleigh wave modes can accurately be picked as the peaks of the modulus of the Green's function (at $k_{\mathrm{R}j}^{\mathrm{Tp}}$) and the attenuation $A_{\mathrm{R}j}^{\mathrm{Th}}$ can be determined with the half power bandwidth method. Figure 4a shows $A_{\mathrm{R}j}^{\mathrm{Tp}}$ $(j = 1, 2)$ up to 100 Hz. A good correspondence is found between $A_{\mathrm{R1}}^{\mathrm{Tp}}$ and $A_{\mathrm{R1}}^{\mathrm{T}}$. For the second mode, a good correspondence between $A_{\mathrm{R2}}^{\mathrm{Tp}}$ and $A_{\mathrm{R2}}^{\mathrm{T}}$ is only found for frequencies below 50 Hz.

To account for C_2 in the calculation of the Rayleigh wave phase velocity and attenuation, the circle fit method is proposed (Ewins, 1984). Figure 2b shows the Nyquist plot of $\tilde{u}_{zz}^{G}(k_r,\omega)$ at 50 Hz, mapping the real part against the imaginary part for each wavenumber. In this representation Equation 6 corresponds to a circle. A circle is fitted through $\tilde{u}_{zz}^{G}(k_r,\omega)$ at 50 Hz for wavenumbers close to $k_{\mathrm{R1}}^{\mathrm{T}}$. $|C_1/(2\xi_{\mathrm{R1}})|$ is the diameter of the circle. C_2 causes a shift of the circle in the complex plane, thereby altering the location and shape of the peak of the modulus of the Green's function. If for example the centre of the circle would be shifted to the origin of the complex plane, there would be no peak and all points would have the same modulus.

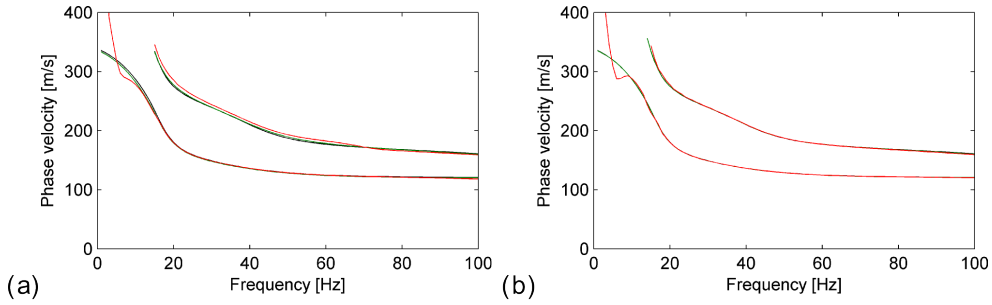

Figure 3. $C_{\mathrm{R}j}^{\mathrm{T}}$, $(j = 1, 2)$ (black) and (a) $C_{\mathrm{R}j}^{\mathrm{Tp}}$ (green) and $C_{\mathrm{R}j}^{\mathrm{Ep}}$ (red) determined by peak picking, and (b) $C_{\mathrm{R}j}^{\mathrm{Tc}}$ (green) and $C_{\mathrm{R}j}^{\mathrm{Ec}}$ (red) determined by the circle fit method.

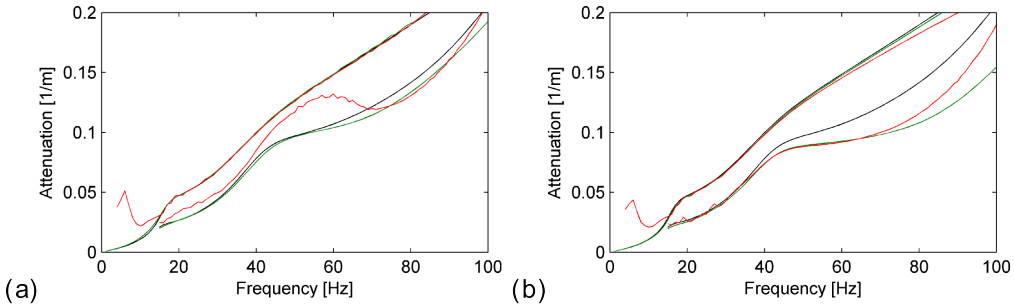

Figure 4. $A_{\mathrm{R}j}^{\mathrm{T}}$ (black), $(j = 1, 2)$ and (a) $A_{\mathrm{R}j}^{\mathrm{Th}}$ (green) and $A_{\mathrm{R}j}^{\mathrm{Eh}}$ (red) determined by the half-power bandwidth method, and (b) $A_{\mathrm{R}j}^{\mathrm{Tc}}$ (green) and $A_{\mathrm{R}j}^{\mathrm{Ec}}$ (red) determined by the circle fit method.

$k_{\mathrm{R}1}^{\mathrm{Tc}}$ is the wavenumber which maximizes the angular sweep $\mathrm{d}\theta/k_r$, where θ is the phase of the Green's function with respect to the circle centre and a reference (horizontal) line, marked green in figure 2. For comparison, $\tilde{u}_{zz}^{G}\left(k_{\mathrm{R}1}^{\mathrm{T}}, \omega\right)$ at 50 Hz is marked in black. This procedure is used to determine $C_{\mathrm{R}j}^{\mathrm{Tc}}$ $(j = 1, 2)$ for frequencies up to 100 Hz, shown in figure 3b. A comparison with figure 3a shows that $C_{\mathrm{R}j}^{\mathrm{Tc}}$ are more accurate than $C_{\mathrm{R}j}^{\mathrm{Tp}}$.

The attenuation can be determined as:

$$A_{\mathrm{R}j}^{\mathrm{Tc}} = \frac{k_a^2 - k_b^2}{2k_{\mathrm{R}j}^{\mathrm{Tc}}[\tan(\alpha_a/2) + \tan(\alpha_b/2)]}, \tag{7}$$

where k_a and k_b are wavenumbers larger and smaller than $k_{\mathrm{R}j}^{\mathrm{Tc}}$, respectively, and α_a and α_b are the corresponding angles on both sides of $k_{\mathrm{R}j}^{\mathrm{Tc}}$ with respect to the centre of the circle. Different pairs k_a and k_b can be used to obtain an averaged $A_{\mathrm{R}j}^{\mathrm{Tc}}$. The Rayleigh wave phase velocity and attenuation obtained with the circle fit method are independent of the value of C_2. Figure 4b shows $A_{\mathrm{R}j}^{\mathrm{Tc}}$ $(j = 1, 2)$ for frequencies up to 100 Hz. A good correspondence is found between $A_{\mathrm{R}1}^{\mathrm{Tc}}$ and $A_{\mathrm{R}1}^{\mathrm{T}}$. A good correspondence between $A_{\mathrm{R}2}^{\mathrm{Tc}}$ and $A_{\mathrm{R}2}^{\mathrm{T}}$ is only found for frequencies below 30 Hz. A comparison with figure 4a shows that, for this site, $A_{\mathrm{R}j}^{\mathrm{Th}}$ are more accurate than $A_{\mathrm{R}j}^{\mathrm{Tc}}$.

Simulation of a field experiment

In an active MASW experiment, the soil is often excited by a hammer impact or a drop weight on a foundation. From the vibration response at different receiver locations, an experimental fk-spectrum can be obtained. Instead of performing a real experiment, a vertical displacement field resulting from a spatial and temporal Dirac impulse load is simulated. Based on the analytical fk-spectrum of $\tilde{u}_{zz}^{G}(k_r, \omega)$ shown in Figure 1a, the response $\hat{u}_{zz}^{G}(r, \omega)$ in the frequency-space domain is obtained by an inverse Hankel transform, to account for the cylinder symmetry of the wavefronts. This transformation is partially performed analytically and numerically (Schevenels, 2007), with 5000 wavenumbers logarithmically sampled between $\omega \times 10^{-8}$ and $\omega \times 10^{4}$ [rad/m] for each frequency. Next, $\hat{u}_{zz}^{G}(r, \omega)$ is discretized according to a realistic receiver array with a length of 100 m and a receiver distance of 1 m. These samples are not shown here, but are used in a truncated forward Hankel transform, to obtain the experimental fk-spectrum of $\tilde{u}_{zz}^{G}(k_r, \omega)$. Following Forbriger (2003), the Bessel function $J_0(k_r r)$ is replaced by the zeroth order Hankel function $H_0^{(1)}(k_r r)/2$ of the first kind to reduce aliasing by accounting for the fact that the wave field consists of outgoing waves only. The following transformation is obtained:

$$\tilde{u}_{zz}^{G}(k_r, \omega) = \frac{1}{2} \int_0^{r_{\max}} \hat{u}_{zz}^{G}(r, \omega)\, H_0^1(k_r r) \mathrm{d}r. \tag{8}$$

The integral is evaluated using a generalized Filon quadrature (Frazer and Gettrust, 1984), using linear interpolation. Figure 5a shows the experimental fk-spectrum of the Green's function at the site in Lincent, normalized for each frequency, as a function of frequency ω and phase velocity $C_r = \omega / k_r$. It can be seen that the truncation of the integral in Equation 8 results in a widening of the Rayleigh peak, called leakage, at low frequencies in the fk-spectrum and consequently an overestimation of the attenuation coefficient. In order to mitigate this effect, a window $\hat{w}(r, \omega) = e^{-A_{\mathrm{art}}(\omega) r}$ that decays exponentially with the distance r is applied to the data in the frequency-space domain, when calculating the attenuation. A similar windowing technique is commonly used in mechanical and structural dynamics to determine the damping ratio of weakly damped systems from a free vibration signal with a limited length in time (Fladung and Rost, 1997). The application of an exponential window can be considered as the introduction of artificial damping, resulting in a stronger spatial decay of the surface waves. This needs to be compensated for when calculating the attenuation. The decay rate is determined by $A_{\mathrm{art}}(\omega)$. For each frequency $A_{\mathrm{art}}(\omega)$ is chosen as the smallest positive value that satisfies the following inequality:

$$A_{\mathrm{art}}(\omega) = \frac{\hat{w}(r_{\max}, \omega) \hat{u}_{zz}^{G}(r_{\max}, \omega)}{\hat{w}(r_{\min}, \omega) \hat{u}_{zz}^{G}(r_{\min}, \omega)} \leq q, \tag{9}$$

where $r_{\min}$ and $r_{\max}$ denote the positions of the nearest and the farthest receiver, respectively. The application of the window ensures that the amplitude ratio of the response at the farthest and the nearest receiver does not exceed a value q. The optimal value of q depends on the receiver setup. Badsar et al. (2010) recommend a value of $q = 10^{-4}$ for the setup used here. The attenuation coefficient obtained for the different modes is affected by the exponential window $\hat{w}(r, \omega)$. The values of $A_{\mathrm{R}j}^{\mathrm{Eh}}(\omega)$ or $A_{\mathrm{R}j}^{\mathrm{Ec}}(\omega)$ are retrieved by subtracting the artificial attenuation coefficient $A_{\mathrm{art}}(\omega)$.

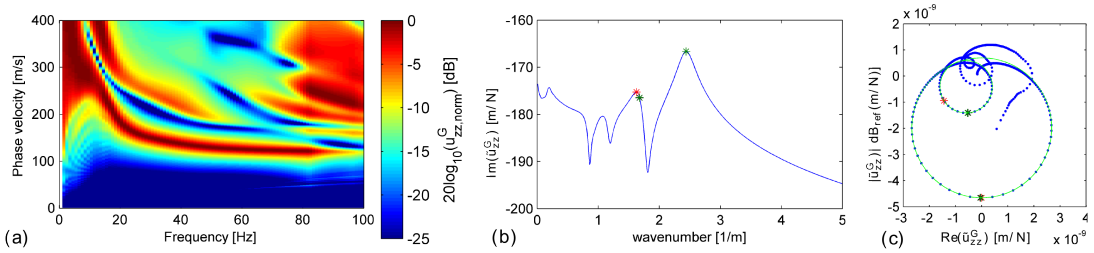

Figure 5. Experimental (a) fk-spectrum of the Green's function at the site in Lincent, (b) modulus and (c) Nyquist plot of the Green's function $\tilde{u}^G_{zz}(k_r, \omega)$ at 50 Hz.

The experimental fk-spectrum is now used to obtain $C^{\mathrm{Ep}}_{\mathrm{R}j}$ with peak picking, $A^{\mathrm{Eh}}_{\mathrm{R}j}$ with the half-power bandwidth method and $C^{\mathrm{Ec}}_{\mathrm{R}j}$ and $A^{\mathrm{Ec}}_{\mathrm{R}j}$ with the circle fit method, for the first two modes for frequencies up to 100 Hz. Figure 5b and 5c show the modulus and Nyquist plot of the experimental Green's function $\tilde{u}^G_{zz}(k_r, \omega)$ at 50 Hz, respectively. A comparison with the theoretical Green's function in figure 2, shows that the experimental function is affected by the spatial sampling of the MASW experiment. The black markers correspond to $k^{\mathrm{T}}_{\mathrm{Rj}}$, the red to $k^{\mathrm{Ep}}_{\mathrm{R}j}$ and the green to $k^{\mathrm{Ec}}_{\mathrm{Rj1}}$. The circle of the second mode is shifted towards the origin of the complex plane, which results in a shift and a widening of the peak, explaining the less accurate estimates of phase velocity and attenuation obtained by the peak picking and half-power bandwidth method for the second mode. The circle fit method is not influenced by the shift of the circle.

Figure 3a shows a comparison between $C^{\mathrm{T}}_{\mathrm{R}j}$, $C^{\mathrm{Tp}}_{\mathrm{R}j}$ and $C^{\mathrm{Ep}}_{\mathrm{R}j}$ obtained with peak picking. A good fit is found between the experimental dispersion curve $C^{\mathrm{Ep}}_{\mathrm{R1}}$ and both theoretical dispersion curves $C^{\mathrm{T}}_{\mathrm{R1}}$ and $C^{\mathrm{Tp}}_{\mathrm{R1}}$ for frequencies above 15 Hz, even for frequencies where aliasing occurs. For $C^{\mathrm{Ep}}_{\mathrm{R2}}$, a deviation up to 5 m/s is found with $C^{\mathrm{T}}_{\mathrm{R2}}$ or $C^{\mathrm{Tp}}_{\mathrm{R2}}$. Figure 3b shows a similar comparison between $C^{\mathrm{T}}_{\mathrm{R}j}$, $C^{\mathrm{Tc}}_{\mathrm{R}j}$ and $C^{\mathrm{Ec}}_{\mathrm{R}j}$ obtained with the circle fit method. For both modes the circle fit method is more accurate than the peak picking method.

Figure 4a shows a comparison between $A^{\mathrm{T}}_{\mathrm{R}j}$, $A^{\mathrm{Th}}_{\mathrm{R}j}$ and $A^{\mathrm{Eh}}_{\mathrm{R}j}$ obtained with the half-power bandwidth method. There is a good correspondence between the experimental curve $A^{\mathrm{Eh}}_{\mathrm{R1}}$ and the theoretical curves $A^{\mathrm{T}}_{\mathrm{R1}}$ and $A^{\mathrm{Th}}_{\mathrm{R1}}$ for frequencies between 15 and 80 Hz. For the second mode, the half-power bandwidth method performed on the experimental fk-spectrum is affected by the discretization and truncation of the Hankel transform and, although there is a reasonable fit between $A^{\mathrm{Th}}_{\mathrm{R2}}$ and $A^{\mathrm{T}}_{\mathrm{R2}}$, there is no good fit between $A^{\mathrm{Eh}}_{\mathrm{R2}}$ and any of the two theoretical curves. Figure 4b shows a comparison between $A^{\mathrm{T}}_{\mathrm{R}j}$, $A^{\mathrm{Tc}}_{\mathrm{R}j}$ and $A^{\mathrm{Ec}}_{\mathrm{R}j}$ obtained with the circle fit method. There is a good correspondence between the experimental curve $A^{\mathrm{Ec}}_{\mathrm{R1}}$ and the theoretical curves $A^{\mathrm{T}}_{\mathrm{R1}}$ and $A^{\mathrm{Tc}}_{\mathrm{R1}}$ for frequencies between 15 and 80 Hz. For the higher frequencies, the estimate $A^{\mathrm{Eh}}_{\mathrm{R1}}$ is slightly better. For the second mode, neither $A^{\mathrm{Tc}}_{\mathrm{R2}}$ or $A^{\mathrm{Ec}}_{\mathrm{R2}}$ have a good match with $A^{\mathrm{T}}_{\mathrm{R}j}$ for frequencies above 30 Hz. There is, however, a good fit between $A^{\mathrm{Ec}}_{\mathrm{R2}}$ and $A^{\mathrm{Tc}}_{\mathrm{R2}}$. This means that, although the circle fit method does not result in the exact attenuation curve, the results are less affected by the discretization and truncation of the Hankel transform. $A^{\mathrm{Tc}}_{\mathrm{R}}$ could thus be used as a new, robust measure of Rayleigh wave attenuation during an inversion procedure.

Conclusions

The circle fit method for determination of dispersion and attenuation curves of Rayleigh wave modes of layered halfspaces is presented. Based on the example shown, it is found that this method allows for a better determination of multi-modal dispersion curves than traditional peak picking in the fk-domain. Regarding the determination of attenuation curves, it is found that for higher order, non-dominant Rayleigh wave modes, it is possible to obtain an experimental measure of attenuation, allowing a multi-modal inversion process to determine material damping, which was previously not possible.

Acknowledgments

The first author is a doctoral fellow of the Research Foundation Flanders (FWO). The financial support is gratefully acknowledged.

References

Badsar SA, Schevenels M, Haegeman W, and Degrande G. Determination of the damping ratio in the soil from SASW tests using the half-power bandwidth method. *Geophysical Journal International 2010*; **182**(3): 1493–1508.

Ewins DJ. *Modal testing: theory and practice*. Research Studies Press Ltd., Letchworth, UK, 1984.

Fladung W and Rost R. Application and correction of the exponential window for frequency response functions. *Mechanical Systems and Signal Processing 1997*; **11**(1): 23–36.

Forbriger T. Inversion of shallow-seismic wavefields: I. Wavefield transformation. *Geophysical Journal International 2003*; **153**(3): 719–734.

Foti S. Using transfer function for estimating dissipative properties of soils from surface-wave data. *Near Surface Geophysics 2004*; **2**(4): 231–240.

Foti S, Parolai S, Albarello D, and Picozzi M. Application of surface-wave methods for seismic site characterization. *Surveys in Geophysics* 2011; **32**(6): 777–825.

Frazer LN and Gettrust JF. On a generalization of Filon's method and the computation of the oscillatory integrals of seismology. *Geophysical Journal of the Royal Astronomical Society 1984*; **76**: 461–481.

Kausel E and Roësset JM. Stiffness matrices for layered soils. *Bulletin of the Seismological Society of America 1981*; **71**(6): 1743–1761.

Lai GC, Rix GJ, Foti S, and Roma V. Simultaneous measurement and inversion of surface wave dispersion and attenuation curves. *Soil Dynamics and Earthquake Engineering 2002*; **22**(9-12): 923–930.

Misbah AS and Strobbia CL. Joint estimation of modal attenuation and velocity from multichannel surface wave data. *Geophysics 2014*; **79**(3): 25-38.

Park CB, Miller RD, and Xia J. Multichannel analysis of surface waves. *Geophysics 1999*; **64**(3): 800–808.

Rizzo FJ and Shippy DJ. An application of the correspondence principle of linear viscoelasticity theory. *SIAM Journal on Applied Mathematics 1971*, **21**(2): 321–330.

Schevenels M, *The impact of uncertain dynamic soil characteristics on the prediction of ground vibrations*. Ph.D. thesis, Department of Civil Engineering, KU Leuven, 2007

Schevenels M, François S, and Degrande G. EDT: An ElastoDynamics Toolbox for MATLAB. *Computers & Geosciences* 2009; **35**(8): 1752–1754.

Xia J, Miller RD, Park CB, and Tian G. Determining Q of near-surface materials from Rayleigh waves. *Journal of Applied Geophysics 2002*, **51**(2-4):121–129.